Proceedings of ASME Turbo Expo 2011
GT2011
June 6-10, 2011, Vancouver, British Columbia, Canada

GT2011-46617

THE EFFECTS OF CONJUGATE HEAT TRANSFER ON THE THERMAL FIELD ABOVE A FILM COOLED WALL

JASON E. DEES*
The University of Texas at Austin
Austin, Texas USA

DAVID G. BOGARD
The University of Texas at Austin
Austin, Texas USA

GUSTAVO A. LEDEZMA
GE Global Research Center
Niskayuna, NY USA

GREGORY M. LASKOWSKI
GE Global Research Center
Niskayuna, NY USA

ABSTRACT

Common gas turbine heat transfer analysis methods rely on the assumption that the driving temperature for heat transfer to a film cooled wall can be approximated by the adiabatic wall temperature. This assumption implies that the gas temperature above a film cooled adiabatic wall is representative of the overlying gas temperature on a film cooled conducting wall. This assumption has never been evaluated experimentally. In order for the adiabatic wall temperature as driving temperature for heat transfer assumption to be valid, the developing thermal boundary layer that exists above a conducting wall must not significantly affect the overriding gas temperature. In this paper, thermal fields above conducting and adiabatic walls of identical geometry and at the same experimental conditions were measured. These measurements allow for a direct comparison of the thermal fields above each wall in order to determine the validity of the adiabatic wall temperature as driving temperature for heat transfer assumption. In cases where the film cooling jet was detached, a very clear effect of the developing thermal boundary layer on the gas temperature above the wall was measured. In this case, the temperatures above the wall were clearly not well represented by the adiabatic wall temperature. For cases where the film cooling jet remained attached, differences in the thermal fields above the adiabatic and conducting wall were small, indicating a very thin thermal boundary layer existed beneath the coolant jet.

*Currently at GE Global Research Center

INTRODUCTION

The design of turbine hot gas path components must account for the fact that modern engines operate at temperatures well beyond the allowable material limit. In order to keep hot gas path components within their allowable operating range, complicated active cooling schemes are implemented. Cooling schemes employed in gas turbine airfoil design include internal convective cooling as well as external film cooling. In order to accurately predict the life of a turbine blade or vane for a given cooling configuration, detailed information concerning the metal temperatures is necessary.

Testing cooling configurations on an operating engine is not only expensive, but obtaining quality component metal temperature data is extremely difficult due to the extreme operating conditions and difficulty in accessing the areas of interest. For these reasons, gas turbine cooling designers have relied on an analysis which relies on decoupling the internal and external flow fields through the use of a known wall condition, typically an adiabatic wall. With the internal and external cooling problems separated, detailed parametric studies can be undertaken with the goal of optimizing the internal and external cooling schemes. These tests have the benefit of simplifying the analysis as well as being relatively inexpensive. Internal cooling studies typically focus on maximizing the internal convective heat transfer coefficient for a given coolant flow. External cooling focuses on film cooling and the associated film effectiveness, or film coverage on the component surface, as well as quantification of the external convective heat transfer coefficient. The component metal temperature, which is the figure of merit, can then be solved for using experimentally measured internal and external cooling parameters as boundary conditions for FEM codes.

Metal temperatures calculated in the way described previously rely on accurate boundary conditions, which are subject to simplifying assumptions. One way in which the boundary condition accuracy can be brought into question is through the common assumption that T_{aw} is the appropriate driving temperature for external heat transfer. The use of T_{aw} as the driving temperature for heat transfer, as seen in Equation 1, was first proposed by Goldstein [1].

$$h_f = \frac{q''}{T_{aw} - T_w} \quad (1)$$

Intuitively, a strong case can be made for use of the adiabatic wall temperature in heat transfer coefficient definition because it should represent the overriding gas temperature of the film cooled wall. For example, on areas of the wall where little film cooling exists, such as the midline between two film cooling holes, the adiabatic wall temperature is equal to or very close to the mainstream temperature since there is virtually no coolant gas over that location. Directly behind a film cooling hole, the adiabatic wall temperature will be some value between the coolant exit temperature and mainstream temperature, dependent on the amount of mixing between the coolant jet and the mainstream gas. While Goldstein [1] states that the film cooling heat transfer coefficient defined in Equation 1 should be independent of the coolant temperature, no proof is given. A second heat transfer coefficient could be defined by using the mainstream temperature in place of T_{aw}, however this heat transfer coefficient would clearly vary strongly with coolant temperature.

Although arguments for the use of T_{aw} as the driving temperature for heat transfer can be made, virtually no critical evaluation of this assumption can be found in the open literature. Choe et al. [2] analytically evaluated the heat flux into a film cooled wall using a superposition analysis. For the hypothetical conducting constant temperature wall examined in Choe et al. [2], the adiabatic wall temperature predicted using Equation 1 and the predicted heat flux on the conducting wall would not be the same as the adiabatic wall temperature measured directly from an adiabatic surface.

Two different studies by Harrison and Bogard [3, 4] attempted to evaluate the adiabatic wall temperature as driving temperature assumption using computational tools. In both studies, Fluent was used to compare a fully conjugate prediction of metal temperature and heat flux as well as a prediction of heat flux and surface temperature through a simulation of conventional analysis techniques using an adiabatic wall. The conventional analysis method used the simulated common experimentally produced boundary conditions for a decoupled analysis and then predicted the metal surface temperature using an FEM solver. The geometry studied was a film cooled flat plate. The authors made a specific point of noting that use of the adiabatic wall temperature to predict heat flux or surface temperature for a conducting component ignores any effects of conjugate heat transfer that may be present. On a conducting wall, a developing thermal boundary layer will be present, and the relative thickness of this boundary layer to the coolant jet thickness has the potential to significantly affect the validity of the adiabatic wall as driving temperature assumption.

Figure 1, taken from Harrison and Bogard [3], presents how the hypothetical developing thermal boundary layer on a film cooled wall may affect the validity of the use of the adiabatic wall temperature as the driving temperature for heat transfer. For a thermal boundary layer that is relatively thin, the overriding gas temperature would be relatively close to the core jet temperature for an attached jet, and T_{aw} would be a reasonable approximation of the driving temperature for heat transfer. For the case of a thick thermal boundary layer, the driving temperature could be any value between the adiabatic wall temperature and mainstream temperature, and probably not well represented by T_{aw}. The results of both studies by Harrison and Bogard [3, 4] showed that where conventional analysis did not predict the surface heat flux temperature accurately, the overriding gas temperatures were not well represented by the adiabatic wall temperature. These differences were solely attributed to conjugate heat transfer effects that are ignored by conventional analysis techniques.

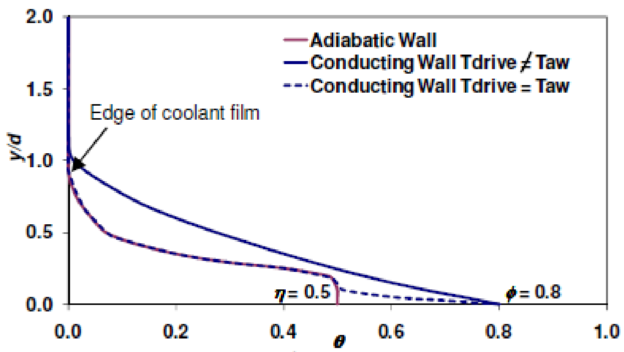

Figure 1: Hypothetical thermal boundary layer profiles demonstrating the validity of T_{aw} as driving temperature [3]

In order to experimentally validate the adiabatic wall temperature as driving temperature for heat transfer assumption, the thermal profile above identical film cooled, conducting and adiabatic components must be measured. While no experimental measurements of thermal profiles above conducting, film cooled walls exists in the open literature, several researchers have measured the thermal profiles above film cooled adiabatic walls. Thole et al. [5] and Coulthard et al. [6] measured thermal profiles above a film cooled, adiabtic flat plate over a wide range of film cooling momentum flux ratios. Measurements of thermal profiles above film cooled, adiabatic vane geometries were performed by Cutbirth and Bogard [7], Waye [8] and Teng et al. [9]. All of the thermal field measurements are useful in understanding the physics of film cooling, however their usefulness in evaluating the adiabatic wall temperature assumption is extremely limited due to their lack of accompanying measurements above a conducting wall. Direct measurement of the thermal field above both adiabatic and conducting film cooled walls is essential in order to experimentally validate the adiabatic wall temperature assumption.

While no experimental measurements of the thermal field above conducting, film cooled walls exist, several studies present surface temperature measurements on conducting walls with and without film cooling. The work of Hylton et al. [10] details surface temperature measurements at the midspan of a scaled up, radially cooled metal turbine vane. Showerhead and main body film cooling was added in follow on studies by Turner et al. [11] and Hylton et al. [12]. The primary goal of studies [10 – 12] was to provide validation data for codes aimed at calculating heat transfer coefficients. No effort was made to produce scaled non-dimensional surface temperatures that were representative of engine components.

A critical aspect in matching the developing boundary layer growth, which is necessary to evaluate the effect of the boundary layer on the adiabatic wall temperature assumption, is matching the non-dimensional surface temperature distribution on the test vane to the engine condition. Sweeney and Rhodes [13] developed a matched *Bi* model in order to simulate the overall cooling performance of Lamilloy, which uses effusion cooling and a double wall with extensive internal cooling. Sweeney and Rhodes used a flat plate that was constructed of a lower thermal conductivity material (relative to the engine) selected to match *Bi* to engine conditions. Matching *Bi*, defined in equation 1 to be the ratio of convection heat transfer resistance to the conduction resistance,

$$Bi = \frac{h_e t}{k} \qquad [1]$$

Matching Bi to the engine condition ensured that the ratio of convective heat transfer at the solid surface to the conduction through the solid matched the engine condition and allowed for direct measurement of non-dimensional metal temperatures that were representative of an engine component. Additional experimental studies utilizing the matched *Bi* were performed by Albert et al. [14] and Mouzon et al. [15], which simulated a conducting leading edge model with internal impingement.

More recently, Dees et al. [16 – 19] performed a series of studies on a scaled up, matched *Bi* vane cooled with an internal cooling circuit designed to be representative of typical internal cooling configurations. The first two studies by Dees et al. [16. 17] detailed surface temperature measurements on an internally cooled vane with and without internal rib turbulators. Dees et al. [18] measured the developing thermal and momentum boundary layers above the internally cooled turbine vane. Surface temperature measurements on identical adiabatic and conducting vanes were measured in Dees et al. [19]. The current study measures the associated thermal fields above the film cooled adiabatic and conducting vanes.

The goal of the current work is to experimentally measure the developing thermal field above film cooled adiabatic and conducting walls. The side by side measurements of the thermal fields above the adiabatic and conducting film cooled walls provides an opportunity for the first experimental evaluation of the commonly held assumption that the adiabatic wall temperature is the appropriate driving temperature for heat transfer to a film cooled wall. By comparing the thermal boundary layer measurements above the adiabatic and conducting walls, the effect of the conducting wall on the overriding gas temperature was evaluated over a range of film cooling rates and distances from film cooling injection.

NOMENCLATURE

Bi	=Biot Number, $\frac{h_e t}{k}$
C	= vane chord length = 56.2 cm
C_p	= pressure coefficient, $\frac{p - p_\infty}{\frac{1}{2}\rho U^2}$
D_h	= coolant channel hydraulic diameter
d	= film cooling hole diameter = 4.2 mm
e	= rib height
h	= heat transfer coefficient
H	= vane span height = 54.7 cm
k	= thermal conductivity
K	= acceleration parameter, $\frac{\nu}{U^2}\frac{dU}{ds}$
t	= thickness of vane wall = 1.27 cm
p	= static pressure, pitch between rib turbulators
q''	= heat flux
Re	= Reynolds number
s	= streamwise surface distance from stagnation
T	= temperature
Tu	= Turbulence Intensity
U	= flow velocity
w	= rib width
x	= streamwise coordinate from downstream edge of film cooling holes
y	= spanwise coordinate
z	=spanwise distance from bottom of vane

<u>Greek</u>

Λ_f	= Turbulence integral length scale
σ	= Stephan-Boltzmann constant
η	= adiabatic effectiveness
ϕ	= Overall effectiveness
θ	= non-dimensionalized gas temperature
ρ	= density
ν	= kinematic viscosity

<u>Subscripts</u>

aw	= adiabatic wall
c	= coolant at test vane coolant circuit inlet
C	= true chord of airfoil
cc	= conduction correction
e	= external
f	= film at film cooling exit
w	= outer wall surface
∞	= freestream

EXPERIMENTAL FACILITIES AND PROCEDURES

All measurements were performed in a closed loop wind tunnel facility at the University of Texas at Austin. The test section was a three vane, two passage linear cascade with a removable center test airfoil. The removable center airfoil allowed for conducting and adiabatic airfoils to be easily interchanged in the test section. The test airfoil geometry was the C3X vane of Hylton et al. [10] scaled up 3.88 times. The test section featured two adjustable bypass flows and an adjustable outer wall designed to set the pressure distribution around the center test vane to that of an infinite cascade. A schematic of the test section is shown in Figure 2.

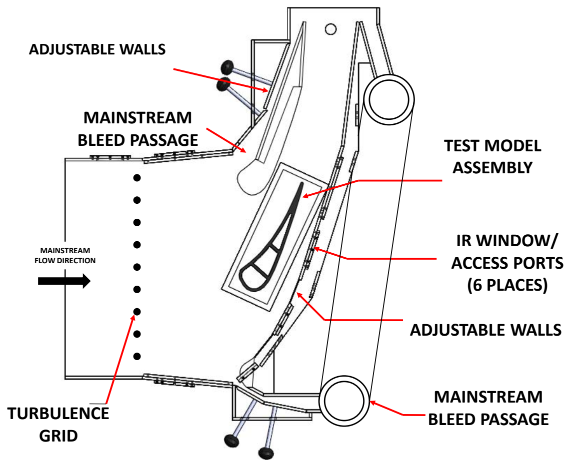

Figure 2: Schematic of the simulated turbine vane test section

The pressure distribution around the test airfoil matched the predicted pressure distribution for an infinite cascade, and is shown in Figure 3. The scaled up test vane had a true chord of C = 56.2 cm and a span height of H =54.7 cm. The pitch between vanes was 45.7 cm. The inlet approach velocity was set so that the Reynolds number based on exit velocity and chord length matched the value of Re = 750,000 stated as the operating condition in Hylton et el. [10]. This produced a uniform inlet velocity of U_∞ = 5.8 m/s.

As stated earlier, the test section was designed so that the center test vane could be easily removed from the test section. This feature allowed for both conducting and near adiabatic vanes to be tested. The adiabatic test vane was constructed out of low conductivity polyurethane foam and had thermal conductivity of k = 0.043 W/m*K. The conducting vane was designed using the matched *Bi* method. In order to properly implement the matched *Bi* method the test vane *Bi* and ratio of internal to external convective heat transfer coefficients must match the engine condition. In order to match *Bi* to the engine conditions, the conducting airfoil was constructed using a castable epoxy resin with thermal conductivity k = 1.02 W/m*K. Matching the ratio of internal to external heat transfer coefficients was achieved by designing an internal coolant flow circuit that could be adjusted across a wide range of coolant flow rates, allowing the ratio to be "dialed in" to the desired value. It should be noted that *Bi* in the current work references the external heat transfer coefficient, and that an equally valid *Bi* could be defined based on the internal heat transfer coefficient. Matching the ratio of the external and internal heat transfer coefficients in addition to one of the possible *Bi* values effectively matches both values of *Bi*. The targeted range of *Bi* was $0.3 < Bi < 0.6$ as described in Dees et al. [16]. A U-bend channel with a single 180° turn was used to cool the forward portion of the vane. A radial cooling channel was used to cool the middle portion of the vane. The trailing edge and aft regions of the vane were uncooled. A schematic of the internal coolant flow circuit is shown in Figure 4. Both the adiabatic and conducting vanes used the same internal coolant flow loop. Additionally, the internal flow loop used in the current study matches the geometry of Dees et al. [16 - 19]. More details on the design and geometry of the internal coolant circuit can be found in [16].

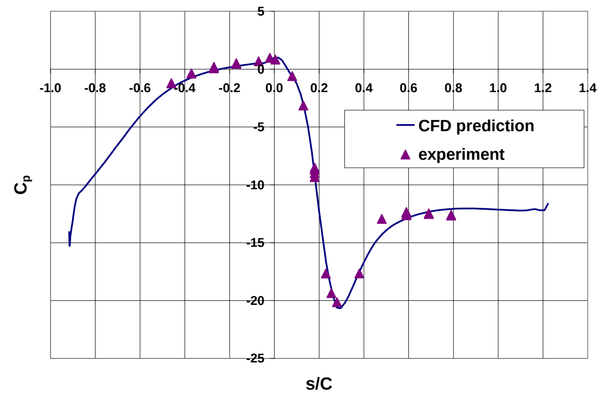

Figure 3: Test airfoil pressure distribution (from [9])

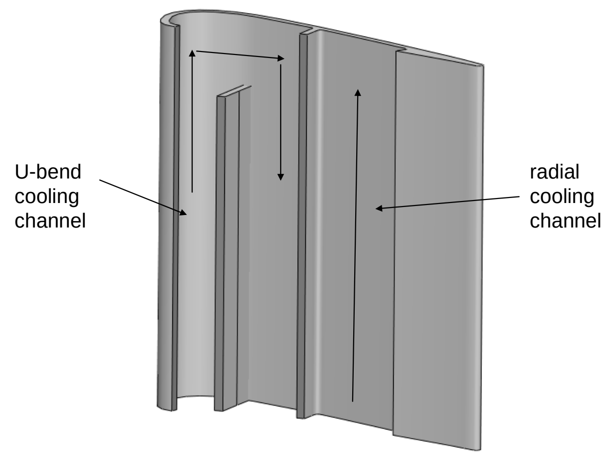

Figure 4: Test airfoil Schematic

A row of cylindrical film cooling holes were installed on the suction side of both test vanes. The film cooling holes were located at a streamwise location of s/C = 0.21 and had a streamwise injection angle of α = 42°. The film cooling holes had a diameter of 4.2mm and a pitch to diameter ratio of 3. A schematic of the test vane showing the location of the suction side film cooling holes is shown in Figure 5.

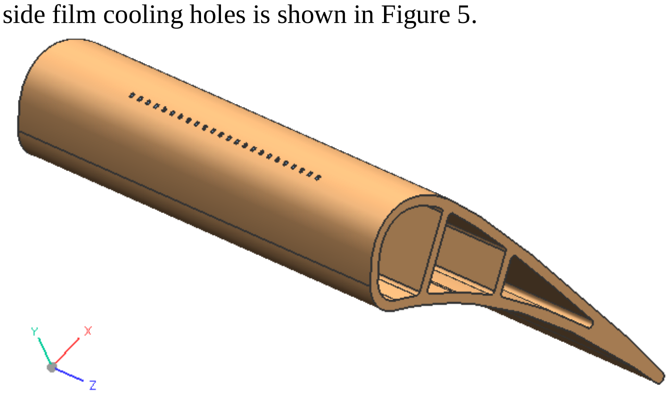

Figure 5: Suction Side Film Cooling Holes

Coolant was supplied to the test vane internal coolant flow loop and film cooling holes via a secondary flow loop. The secondary flow bypassed a portion of the mainstream coolant air through a series of heat exchangers, flow meters, and flow control valves in order to regulate the coolant flow rate and the coolant temperature. Liquid nitrogen was used to cool the secondary flow down to the desired temperature. The flow control valves and flow meters were used to control the coolant flow rates through the U-bend and radial flow channels independently of each other. On the downstream side of the U-bend channel, which fed the suction side film cooling holes, a downstream control valve allowed for the pressure in the test vane to be adjusted. Adjustment of the pressure in the test vane allowed for the film cooling blowing ratio to be controlled independently of the flow through the U-bend circuit. A schematic of the secondary (coolant) flow loop can be seen in Figure 6.

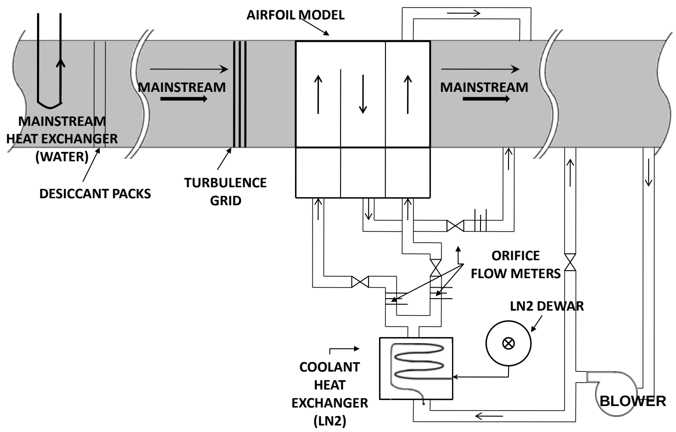

Figure 6: Schematic of secondary flow loop

Gas temperature measurements above the film cooled conducting and adiabatic walls were measured using a microthermocouple probe. The sensing area of the probe consisted of butt-welded E-type thermocouple wires. Measurements were performed on both test airfoils at an internal coolant flow Reynolds number of Re = 20,000 and film cooling momentum flux ratios of I = 0.34, 0.75, and 1.41. All measurements were performed at a coolant to mainstream density ratio of DR = 1.2. In order to eliminate frost formation in the coolant flow circuit and on the test vane surface, the wind tunnel was dried using a gaseous nitrogen purge and desiccant prior to any data being taken.

Measurements were taken at downstream distances of x/d = 1, 3, 5, 10, and 19. A key aspect of making the thermal field measurements was accurate location of the test vane wall. First, the probe was manually moved to within 1mm of the wall, at which point it was bolted to a traverse system that allowed for precise movement normal to the wall and along the vane span. At this time, the probe was carefully moved into the vane wall until the probe was just touching the vane wall. This position was defined to be y = 0. The probe was then adjusted in the spanwise direction (z) in order to line the probe up with the centerline of the film cooling hole, which was defined to be z = 0. This procedure identified the coldest gas temperature at the wall, and therefore may not necessarily identify the coldest gas temperature in the core of the jet. This position was defined by scanning in the z direction until the coldest temperature in the film cooling jet was located. The jet centerline was defined independently for each downstream position. Centerline thermal profile measurements were then performed by incrementally moving the probe away from the wall and taking mean temperature measurements at discreet distances from the wall. For select cases, the entire jet profile was measured, which required moving the probe in the wall normal direction as well as the spanwise direction.

The mean temperature profiles obtained were normalized as shown in Equation 2.

$$\theta = \frac{T_\infty - T_{probe}}{T_\infty - T_f} \qquad (2)$$

For the case of an adiabatic wall, Equation 2 will produce a normalized temperature at the wall (θ_w) that is equivalent to the adiabatic effectiveness (η). For a conducting wall, θ_w is close to but not equal to the overall effectiveness, ϕ. The difference between θ_w and ϕ is related to the difference between the coolant inlet temperature and the film temperature. If the film temperature in Equation 2 was replaced with the vane coolant inlet temperature, the normalized temperature at the wall would be equivalent to the overall effectiveness. Detailed maps of the normalized wall temperature downstream of the film cooling holes were measured for all test cases presented in the current study and are presented in Dees et al. [19].

The uncertainty in normalized thermal profile measurements above the conducting wall was quantified using a statistical analysis of eight repeated thermal profiles above a film cooled conducting wall. This analysis produced a 95% confidence uncertainty in normalized temperature of $\delta\theta = \pm 0.058$ at the wall. A statistical analysis of six repeated profiles above a film cooled adiabatic wall produced an uncertainty in normalized temperature of $\delta\theta = \pm 0.05$ at the wall. Far away from the wall, profiles were repeatable to much greater accuracy than what was seen at the wall.

RESULTS

The thermal profiles measured above the film cooled adiabatic wall at the centerline of a film cooling hole at momentum flux ratios of I = 0.34, 0.75, and 1.41 are presented in Figures 7 – 9, respectively. For all three test conditions thermal profiles were measured at downstream positions of x/d = 1, 3, 5, 10, and 19. Figure 7 shows that for I = 0.34, the thermal profiles suggest that the film cooling jet generally remained attached to the vane surface. At x/d = 1, the coldest part of the film cooling jet was at nominally y/d = 0.2, which indicated a slight separation immediately after film coolant injection. This separation region had disappeared by x/d = 3, indicating that the separated jet had reattached to the surface. For y/d < 0.8, the jet coolant temperature monotonically decreased with increasing x/d, which was consistent with contours of adiabatic effectiveness. This decrease in jet temperature was due to the jet mixing with the warm mainstream. The jet mixing also caused the thickness of the thermal profiles to grow slightly as downstream distance increased. For x/d < 5, the influence of the coolant jet extended to about y/d = 1. For x/d = 10 and x/d = 19, the influence of the jet extended to about y/d = 1.2 and y/d = 1.8, respectively. This thickening of the thermal profile was also attributable to mixing with the mainstream flow and entrainment of hot gas into the film cooling jet.

The thermal profiles for the adiabatic wall at I = 0.75, shown in Figure 8, indicate that the jet was detached for all measurement locations. At x/d = 1 the coldest part of the thermal profile was measured to be at about y/d = 0.6, indicating that the jet was significantly detached. At x/d = 3 the distance from the wall to the coldest part of the jet had decreased to about y/d = 0.3, indicating that slight reattachment occurred between x/d = 1 and x/d = 3. For x/d > 3, the level of jet separation increased with increasing x/d which is typical for a detached jet on a flat surface.

For I = 1.41, shown in Figure 9, similar trends were seen. The jet was detached for all measurement locations. For x/d = 3, temperatures for y/d < 0.4 were somewhat colder than the corresponding temperatures at x/d = 1. Even though the distance of the coldest temperatures from the wall were roughly equivalent for x/d = 1 and x/d =3, very close to the wall colder temperatures were seen at x/d = 3. This can be explained either through slight jet reattachment or dispersion of the cooling jet between the x/d = 1 and x/d = 3 positions. Interestingly, the temperatures at the wall were nearly identical for x/d = 1 and x/d = 3, even though the thermal profile slightly above the wall was colder for the x/d = 3 case. At x/d = 10 and x/d = 19 for I = 1 and I = 1.41, distinct local minima and maxima in gas temperature were measured a finite distance from the wall. Immediately above the wall, relatively warm gas temperatures (minimum θ) were measured compared to the wall temperature. Above this region of warm gas, colder gas temperatures were measured, indicating the position of the film cooling jet. One possible explanation for a layer of relatively cold gas near the wall would be a developing thermal boundary layer. However, due to the adiabatic nature of the test surface, this was considered to be an unlikely cause. Another possible explanation could be that the normal pressure gradients due to the strong surface curvature caused some of the lower momentum coolant to be pulled back down to the vane surface.

In all three figures, the temperature gradient appears to be non-zero, which is unexpected for an adiabatic wall. Of course, the actual test surface is not adiabatic, which is one reason for slight temperature gradients at the wall. A more likely explanation for the existence of temperature gradients at the wall is that the region where no temperature gradient exists is smaller than the measurement resolution, due to a new boundary layer starting downstream of film injection.

The open symbols plotted in Figures 7 – 9 represent the average centerline wall temperature measurement at each downstream measurement. These average values were calculated from the surface temperature measurements reported in Dees et al. [19] across several hole diameters. In general, the gas temperature measurements close to the wall agreed reasonable well the temperature measurement on the wall. However, there were large differences between the measured surface temperatures and first gas temperature measurements for both I = 0.75 and I = 1.41 at x/d = 10 and x/d = 19. Due to the near adiabatic nature of the test vane, it is unlikely that the difference in temperature on the wall and slightly above the wall was due to a developing thermal boundary layer. Another possibility was that skewness in the film cooling jet (due to cross-flow at the hole inlet, this is discussed later) caused inaccurate location of the jet centerline. Since the centerline was located by finding the coldest temperature in the core of the jet, the coldest temperature in the core of the jet may not have been coincident with the coldest gas temperature above the wall.

Figure 10 shows a two dimensional contour plot of mean temperatures above the wall for I = 0.75 at x/d = 5. As was expected from the centerline measurement shown in Figure 7, the film cooling jet was clearly separated from the wall for I = 0.75 at x/d = 5. At x/d = 5 the film cooling jet extended to about z/d = ± 0.8, indicating that the film cooling jet was nominally 1.6d wide at this position. Mixing with the mainstream was expected to cause the jet to disperse and widen with increasing downstream distance. The normal pressure gradient resulting from the surface curvature may have also contributed to the jet becoming broader at this position. Figure 10 shows that the profile of the film cooling jet was not symmetric, which was consistent with the asymmetric profiles of adiabatic effectiveness shown in Dees et al. [19]. This implies that the coolant temperature field above the wall would likely also be skewed. Colder temperatures were seen near the wall for positive z/d, which is consistent with the direction of internal crossflow. Outside of the film cooling jet no developing thermal boundary layers were measured, which was expected for the adiabatic wall.

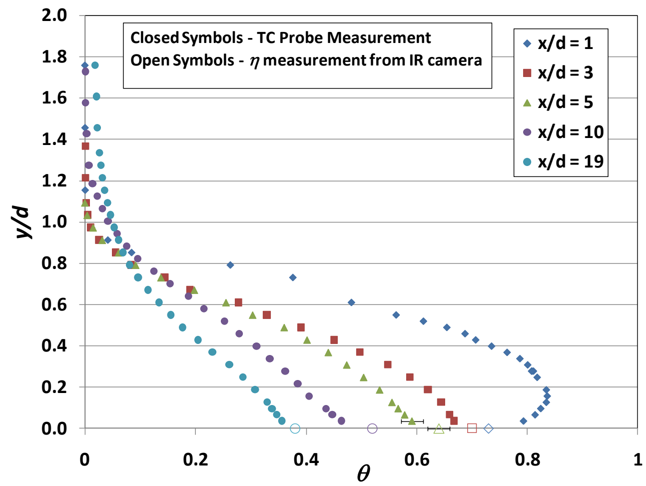

Figure 7: Centerline thermal profile measurements, adiabatic wall, I = 0.34

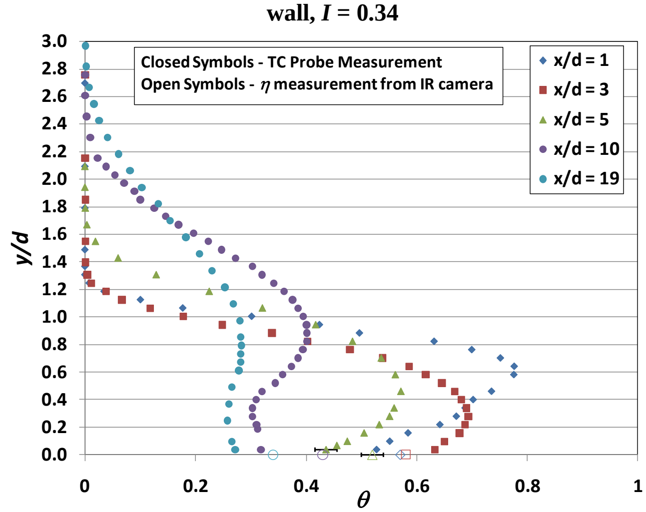

Figure 8: Centerline thermal profile measurements, adiabatic wall, I = 0.75

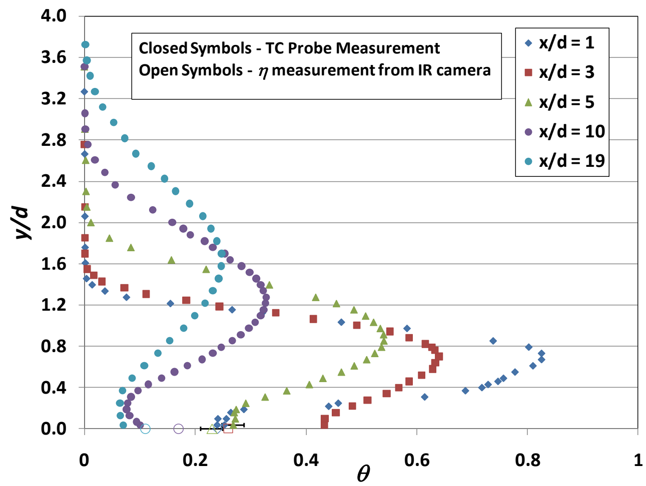

Figure 9: Centerline thermal profile measurements, adiabatic wall, *I* = 1.41

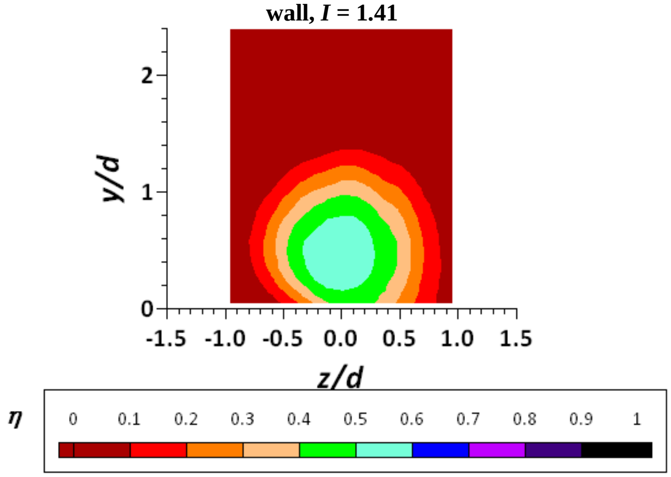

Figure 10: Contour of gas temperature, adiabatic wall, *I* = 0.75, *x/d* = 5

Figure 11 shows some thermal profiles at various spanwise positions extracted from Figure 10. These profiles are useful in order to get a better understanding of the asymmetry that was evident in Figure 10. As the distance from the centerline increased, the gas temperatures decreased everywhere in the film cooling jet. The asymmetry present in the jet can be seen clearly by comparing the positive and negative *z/d* values for the same distance from the centerline. Generally, negative *z/d* had warmer gas temperatures compared to the corresponding positive *z/d* measurement, with the largest differences seen near the wall.

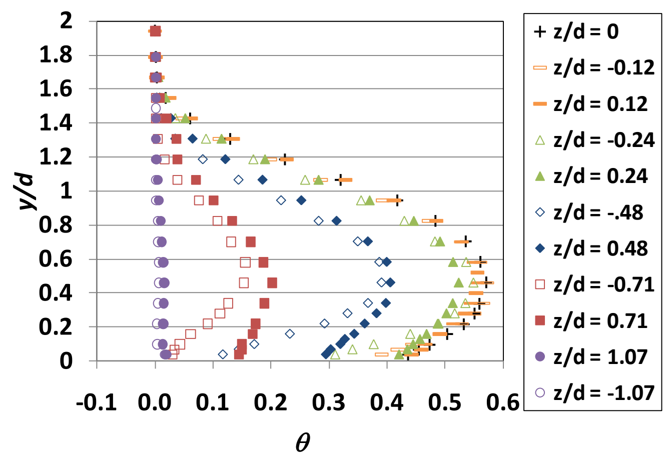

Figure 11: Spanwise gas temperature profiles, adiabatic wall, *I* = 0.75, *x/d* = 5

Figure 12 a contour plot of gas temperature above the adiabatic wall for I = 0.75 and x/d = 10. Relative to Figure 9, the core of the coolant jet temperature was warmer, which was expected due to the jet being mixed out with the freestream gas. The effect of the coolant jet also extended a greater distance away from the wall relative to the x/d = 5 position, which was also seen in the centerline temperature profiles. As was seen at x/d = 5, the profile of the cooling jet was slightly skewed in the direction of the internal crossflow.

Figure 12 shows that some of the coolant gas remained attached to the vane wall while the main jet core was continuing to separate from the surface. This phenomenon explains the increase in θ values seen in the centerline profiles for y/d < 0.2 for I = 0.75 and I = 1.41 at x/d = 10 and x/d = 19. It is possible that the momentum of the coolant gas very near the wall was low enough that the normal pressure gradient due to the surface curvature caused the gas near the wall to remain attached to the surface. Higher velocity fluid in the core of the coolant jet had high enough momentum that the normal pressure gradient was not strong enough to pull the gas back to the vane surface.

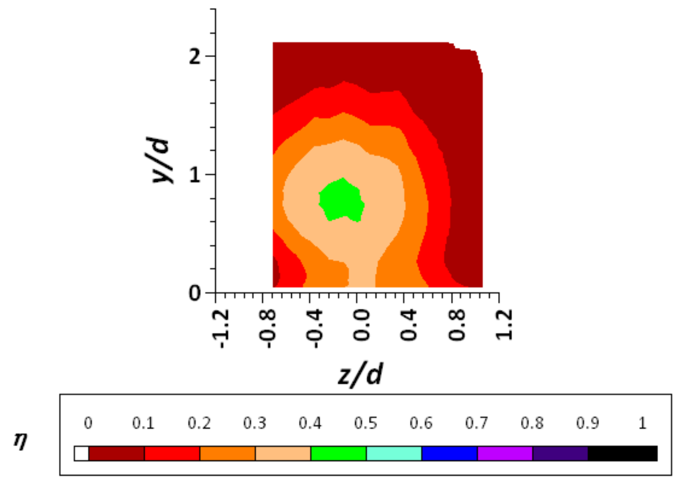

Figure 12: Contour of gas temperature, adiabatic wall, *I* = 0.75, *x/d* = 10

Thermal profiles on the jet centerline at the same conditions presented in Figures 7 – 9 were also measured above the conducting wall. Figures 13 – 15 plot the development of the centerline thermal profiles above the film cooled, conducting wall for I = 0.34, I = 0.75, and I = 1.41, respectively. In a general sense, many of the trends seen in the temperature profiles above the conducting wall were similar to those seen for the adiabatic wall. Increasing the momentum flux ratio increased the level of jet separation and thermal profile thickness. As x/d increased, the temperature in the core of the jet warmed in a very similar manner as what was seen for the adiabatic wall cases, shown in Figures 7– 9. Similar to the adiabatic model, at x/d = 10 and x/d = 19 for I = 0.75 and I = 1.41 a region where $d\theta/dy$ < 0 was seen close to the wall. The thickness of this layer of gas was very similar to that seen on the adiabatic wall. This supports the assertion that the cold gas very close to the wall was likely not due to a developing thermal boundary layer and was more likely due to hydrodynamic effects causing a layer of cold gas to remain very close to the wall.

Also plotted on Figures 13 – 15 is the upstream developing thermal boundary layer that was displaced by the film coolant at film injection. The upstream boundary layer was measured five hole diameters upstream of the film cooling holes and was less than 0.2*d* thick. This boundary layer would be displaced where downstream of the film cooling holes, and a new boundary would start to develop. As can be seen in the similarity of the adiabatic and conducting wall centerline measurements, the effect of the upstream boundary layer appeared to be erased. Very little evidence of a new developing boundary layer on the centerline of the film cooling holes can be seen in Figures 13 – 15, suggesting the new boundary layer is still very thin even 20 hole diameters downstream of injection.

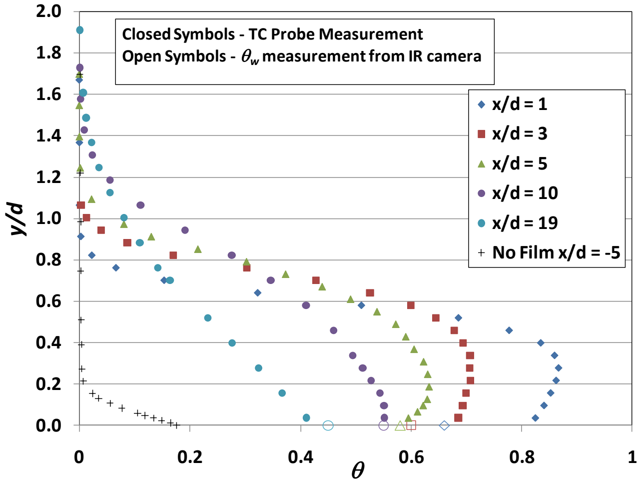

Figure 13: Centerline thermal profile measurements, conducting wall, *I* = 0.34

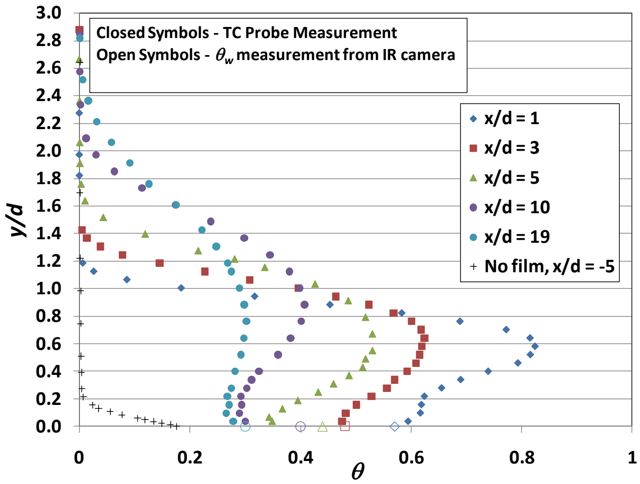

Figure 14: Centerline thermal profile measurements, conducting wall, *I* = 0.75

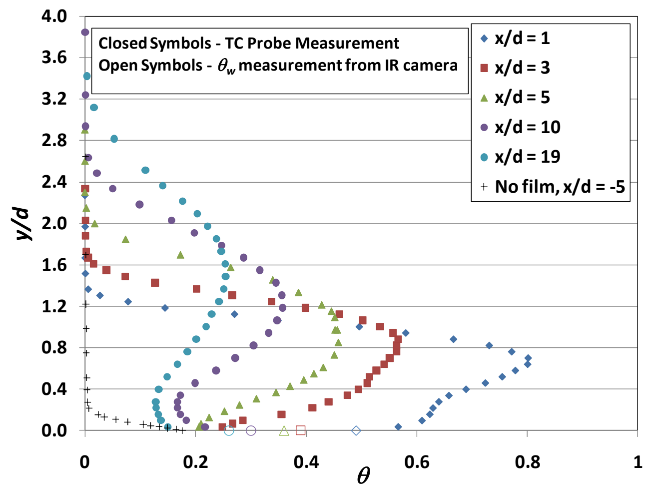

Figure 15: Centerline thermal profile measurements, conducting wall, *I* = 1.41

Figure 16 shows a two dimensional contour of the gas temperature above the wall for I = 0.75 at x/d = 5. Consistent with both centerline profile measurements, Figure 16 shows that the core of the film cooling jet was distinctly separated from the wall for this case. Comparing Figure 16 to Figure 8 shows that there was more separation above the conducting wall compared to the adiabatic wall. Outside of $z/d = \pm 1$, the effect of the developing thermal boundary layer can be seen very close to the wall. The thickness of the developing thermal boundary layer, about 0.2*d*, was consistent with the non-film-cooled measurements at x/d = -5, shown in Figures 13 – 15.

Figure 17 shows coolant profiles taken at various spanwise locations at a streamwise distance of x/d = 5 and I = 0.75. In contrast to the thermal profiles above the adiabatic wall presented in Figures 6 – 8, a developing thermal boundary layer can be clearly seen to exist under the separated film cooling jet for distances away from the centerline larger than 0.48. For distance from the centerline less than 0.48, the developing thermal boundary was very thin. This was consistent with the development of a new thermal boundary layer.

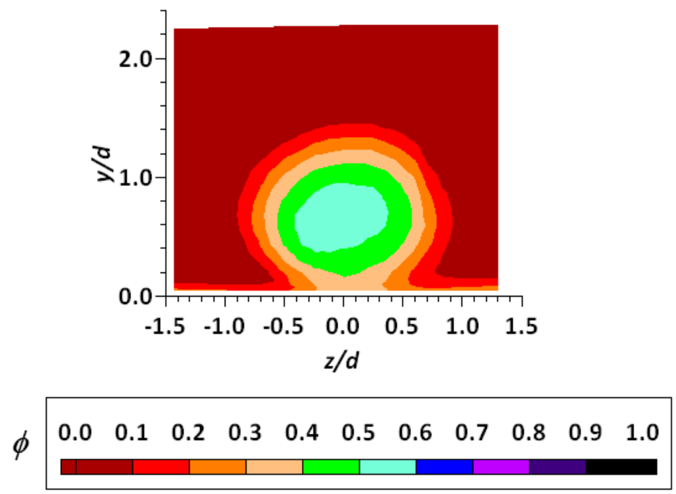

Figure 16: Contour of gas temperature, conducting wall, *I* = 0.75, *x/d* = 5

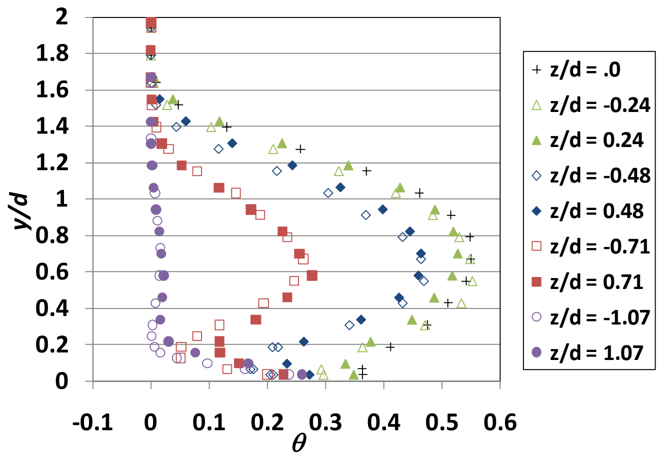

Figure 17: Spanwise gas temperature profiles, conducting wall, *I* = 0.75, *x/d* = 5

In general the thermal fields for the coolant jet above the conducting and adiabatic walls were similar, but for some cases the differences between the conducting and adiabatic models were greater than what was expected. One example of a larger difference between the thermal profiles than expected is presented in Figure 18 which shows a direct comparison of the adiabatic and conducting profiles for $I = 0.34$ at $x/d = 3$. As can be seen in the figure, the thermal profile above the conducting wall was significantly thicker than what was seen above the adiabatic wall. For a given distance from the wall, the gas temperature was also colder above the conducting wall. Due to the thickness of the upstream developing boundary layer on the conducting wall, it was expected that any differences between the adiabatic and conducting thermal fields would be confined to $y/d < 0.2$, about the thickness of the upstream boundary layer. When comparing streamwise development of the thermal profiles shown in Figures 7 and 8 for the adiabatic and conducting walls, respectively, it is evident that the exit profiles at $x/d = 1$ were very similar, with a slight jet separation. But by $x/d = 3$ the coolant jet was drawn back to the wall for the adiabatic wall case and not for the conducting wall case. Another possible explanation for the differences in thermal profiles could be slight differences in the momentum flux ratio between the adiabatic and conducting cases. Slight differences in the film coolant momentum flux ratio could have a significant impact on the resulting film cooling jet thermal field.

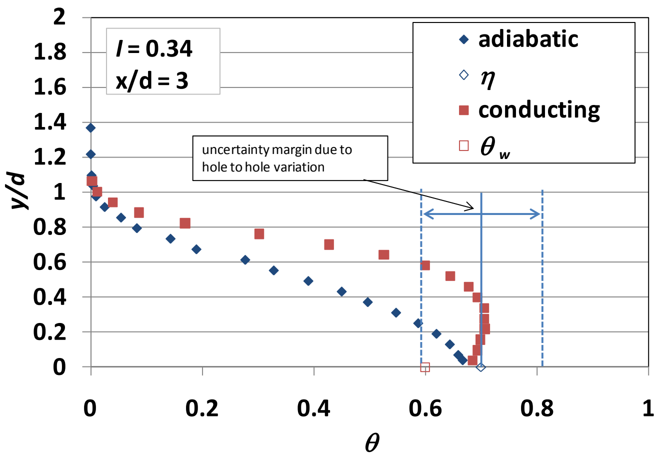

Figure 18: Comparison of centerline thermal profiles, *x/d* = 3, *I* - 0.34

A similar effect was seen for the adiabatic and conducting profiles for $I = 0.75$. Again, at $x/d = 1$ the thermal profiles for the coolant jets for the adiabatic and conducting walls were very similar, but, as shown in Figure 19, by $x/d = 3$ the profiles were distinctly different. Again the difference between the two profiles appears to be due to the coolant jet being drawn back towards the wall for the adiabatic wall case, but not for the conducting wall case. It is not clear what causes this difference in jet reattachment for the adiabatic wall compared to the conducting wall. Again, a possible explanation for this effect could be slight differences in momentum ratio between the two test cases.

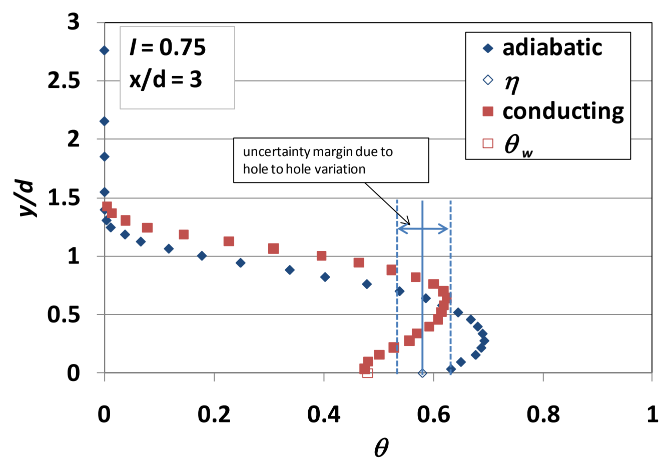

Figure 19: Comparison of centerline thermal profiles, *x/d* = 3, *I* = 0.75

To evaluate whether differences between the conducting and adiabatic walls could be attributed to inherent differences between models and experiments, the hole-to-hole variation and test-to-test variation of the thermal profile measurements were checked. The results of this test are shown in Figure 20. As can be seen in the figure, the repeatability of the measurement behind a single film cooling hole was very good, although there was a slight variation of the thermal profile when moving to a different hole. Comparing the thermal profiles for hole #1 and hole #2, the peak θ values were within 0.03 of each other, and the separation distance from the wall was the same. Near the wall there was more significant difference of $\Delta\theta = 0.06$ between the two holes. These results suggest that the difference in coolant jet separation observed for the adiabatic and conducting wall was not due to experimental uncertainty in momentum flux ratio, since the momentum flux ratio would have been the same for both film holes in the same test. This suggests that while there may have been an effect due to differences in momentum flux ratio between tests, there was also likely a significant effect on temperature profile due to geometric differences between holes on a given airfoil and between holes on the different airfoils.

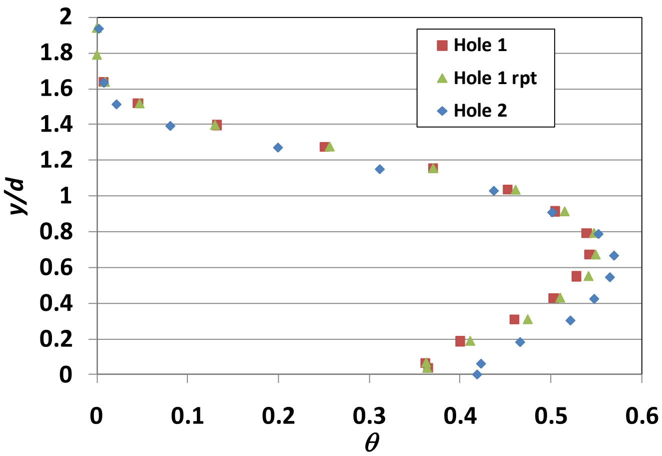

Figure 20: Example of thermal profile variation due to hole to hole variation, x/d = 6, I = 0.75

As mentioned previously, common gas turbine analysis methods rely on the assumption that the adiabatic wall temperature is the appropriate driving temperature for heat transfer to a film cooled wall. For this assumption to be true, the thermal profile above a conducting film cooled wall should have temperature similar to the adiabatic wall temperature. Direct comparisons of the thermal profiles above the conducting and adiabatic walls were made at every experimental condition and are available in Dees [20]. Due to the relatively large uncertainty in adiabatic effectiveness due to hole-to-hole variations, the validity of using adiabatic wall temperature as driving temperature could not be ascertained for many cases. However, one example where the adiabatic wall temperature was clearly a poor assumption for the gas temperature above the conducting wall, and hence a poor assumption as driving temperature for heat transfer, is shown in Figure 21. For I = 1.41, the separated jet drew the cold coolant away from the wall and allowed warmer gas temperatures between the coolant jet and the wall. Figure 20 clearly shows that the temperatures above the conducting wall were colder than the corresponding temperatures above the adiabatic wall. This was likely due to conjugate heat transfer effects with the conducting wall cooling the gas in the near wall region. The conducting wall temperature and gas temperature above the wall for y/d < 0.2 were significantly colder than the corresponding adiabatic wall temperature and gas temperature. The adiabatic wall temperature for I = 1.41 and x/d = 1 was clearly much warmer than the gas temperature above the conducting wall and was not a good choice as driving temperature for heat transfer.

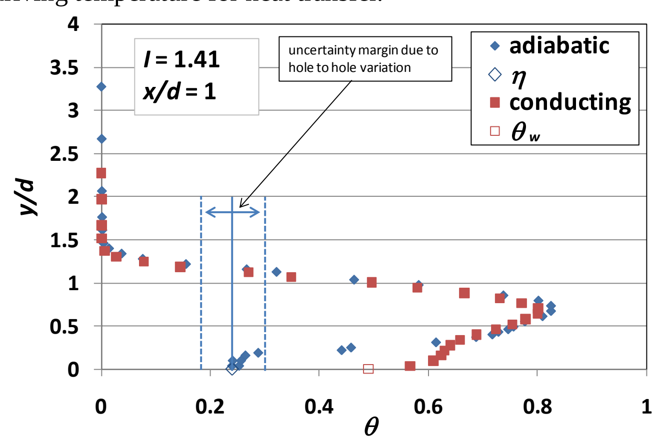

Figure 21: Comparison of centerline thermal profiles, x/d = 1, I = 1.41

CONCLUSIONS

Common gas turbine heat transfer analysis methods rely on the assumption that the adiabatic wall is the appropriate driving temperature for heat transfer to a film cooled wall. This implies that the gas temperature above the wall is unaffected by the developing thermal boundary layer. No experimental evaluation of this assumption has previously been reported. The identical adiabatic and conducting vane geometries in the current study allowed for the first ever evaluation of what impact the developing thermal boundary layer would have on the common presumption that overriding gas at the adiabatic wall temperature drives heat transfer to the wall.

Making a direct comparison of the thermal fields above the conducting and adiabatic walls proved to be more difficult than anticipated. Geometric variations between different film cooling holes caused measurable differences in the thermal profiles above the wall when an identical thermal profile was expected. The associated uncertainties in the thermal profile measurements made drawing specific conclusions concerning the adiabatic wall temperature assumption impossible in many cases. However, valuable insight into the effect of the conducting wall on the overlying gas temperature on a film cooled wall was still gained.

Spanwise contours of mean temperature above a conducting and adiabatic wall with a detached film cooling jet revealed a clear influence of the developing thermal boundary layer on the gas temperature near the wall. Near the edges of the film cooling jet, the developing thermal boundary layer above the conducting wall caused colder temperatures relative to the adiabatic wall. The colder temperatures above the conducting wall were clearly not well represented by the adiabatic wall temperature. At the centerline of the jet, the developing thermal boundary layer was much thinner and the adiabatic wall temperature was a better representation of the overriding gas temperature.

Even though in many cases the developing thermal boundary layer was too thin to cause measurable differences between the conducting and adiabatic cases, it is useful to consider what effect the thin thermal boundary layer would have on the associated heat transfer coefficient. The very thin boundary layer at the jet centerline was a result of the film cooling jet displacing the upstream thermal boundary layer and causing a new thermal boundary layer to develop under the jet. This very thin boundary layer would likely be accompanied by a very strong increase in the heat transfer coefficient relative to a non-film cooled wall. Depending on the exact experimental setup used, reported increases in film cooling heat transfer relative to non film cooled cases can range between a factor of one and two. Experimental methods that ignore upstream heating, which are common in the literature, typically produce little or no increase in the heat transfer coefficient due to film cooling. The very thin thermal boundary layers that existed on the centerline of the film cooling jet downstream of injection relative to the thicker upstream boundary layers magnify the importance of accounting for the upstream heating that takes place on real vanes.

ACKNOWLEDGEMENTS

The authors gratefully acknowledge the support of the NASA NRA program for this research, and the guidance provided by the Technical Monitor Dr. J. Heidmann.

REFERENCES

[1] Goldstein, R.J., 1971, “Film Cooling,” Advances in Heat Transfer, v 7, pp 321 – 379.

[2] Choe, H., Kays, W.M., and Moffat, R.J., 1974, “The Superposition Approach to Film-Cooling,” ASME paper 74-WA/GT-27.

[3] Harrison, K.L. and Bogard, D.G., 2008a, “Evaluation of the Use of the Adiabatic Wall Temperature to Predict Heat Fluxes for Film Cooled Turbine Airfoils,” ISROMAC12-2008-20187.

[4] Harrison, K.L. and Bogard, D.G., 2008b, “Use of the Adiabatic Wall Temperature in Film Cooling to Predict Wall Heat Flux and Temperature,” ASME Paper GT2008-51424.

[5] Thole, K.A., Sinha, A., Bogard, D.G., and Crawford, M.E., 1992, “Mean Temperature Measurements of Jets with a Crossflow for Gas Turbine Film Cooling Application,” Rotating Machinery Transport Phenomena, edited by J.H. Kim and W.J. Wang, Hemisphere, New York, pp. 69 – 85.

[6] Coulthard, S.M., Volino, R.J., and Flack, K.A., 2007, “Effect of Jet Pulsing on Film Cooling – Part I: Effectiveness and Flow-Field Temperature Results,” *Journal of Turbomachinery*, Vol. 129 pp 232 – 246.

[7] Cutbirth, J.M., and Bogard, D.G., 2002, “Evaluation of Pressure Side Film Cooling with Flow and Thermal Field Measurement – Part II: Turbulence Effects,” *Journal of Turbomachinery*, vol. 124 pp 678 – 685.

[8] Waye, S.K., 2005, “Film Cooling Effectiveness of Suction Side Axial Holes, Compound Angle Holes, and Axial Holes Embedded within an Overlying Transverse Trench,” Master’s Thesis, The University of Texas at Austin.

[9] Teng, S., Han, J-C., and Poinsatte, P.E., 2001, “Effect of Film-Hole Shape on Turbine-Blade Film-Cooling Performance,” *Journal of Thermophysics and Heat Transfer*, vol. 15 No. 3.

[10] Hylton, L.D., Milhec, M.S., Turner, E.R., Nealy, D.A., and York, R.E., 1983, “Analytical and Experimental Evaluation of the Heat Transfer Distribution Over the Surface of Turbine Vanes,” NASA CR 168015.

[11] Turner, E.R., Wilson, M.D., Hylton, L.D., and Kaufman, R.M., 1985, “Analytical and Experimental Heat Transfer Distributions with Leading Edge Showerhead Film Cooling,” NASA CR 174827.

[12] Hylton, L.D., Nirmalan, V., Sultanian, B.K., and Kaufman, R.M., 1988, “The Effects of Leading Edge and Downstream Film Cooling on Turbine Vane Heat Transfer,” NASA CR 182133.

[12] Sweeney, P.C., and Rhodes, J.F., “An Infrared Technique for Evaluating Turbine Airfoil Cooling Designs,” *Journal of Turbomachinery*, vol. 122, pp 170 – 177.

[14] Albert, J.E., Bogard, D.G., and Cunha, F., 2004, “Adiabatic and Overall Effectiveness for a Film Cooled Blade,” ASME Paper GT2004-53998.

[15] Mouzon, B.D., Terrel, E.J., Albert, J.E., and Bogard, D.G., 2005, “Net Heat Flux Reduction and Overall Effectiveness for a Turbine Blade Leading Edge,” ASME paper GT2005-69002.

[16] Dees, J.E., Ledezma, G.A., Bogard, D.G., Laskowski, G.M., Tolpadi, A.K., 2009, “Experimental Measurements and Computational Predictions for an Internally Cooled Simulated Turbine Vane,” ASME paper IMECE2009-11622.

[17] Dees, J.E., Ledezma, G.A., Bogard, D.G., Laskowski, G.M., Tolpadi, A.K., 2010, “Experimental and Computational Measurements for an Internally Cooled Simulated Gas Turbine Vane with 90 degree Rib Turbulators,” ASME paper GT2010-23004.

[18] Dees, J.E., Ledezma, G.A., Bogard, D.G., Laskowski, G.M., Tolpadi, A.K., 2010, “Momentum and Thermal Boundary Layer Development on an Internally Cooled Turbine Vane,” ASME paper GT2010-23008.

[19] Dees, J.E., Ledezma, G.A., Bogard, D.G., Laskowski, G.M., Tolpadi, A.K., 2010, “Overall and adiabatic effectiveness values on a scaled up, simulated gas turbine vane: Part I – Experimental Measurements,” ASME paper GT2011-46612.

[20] Dees, J.E., 2010, “Experimental Measurements of Conjugate Heat Transfer on a Scaled-up Gas Turbine Airfoil with Realistic Cooling Configuration,” Ph.D. Dissertation, The University of Texas at Austin.